

**Chemical forms of calcium in Ca,Zn- and Ca,Cd-containing grains  
excreted by tobacco trichomes**

Géraldine Sarret<sup>1</sup>, Marie-Pierre Isaure, Matthew A. Marcus, Emiko Harada,  
Yong-Eui Choi, Sébastien Pairis, Sirine Fakra and Alain Manceau

**Géraldine Sarret, Marie-Pierre Isaure, Emiko Harada and Alain Manceau.** Environmental Geochemistry Group, LGIT, University of Grenoble and CNRS, BP 53, 38041 Grenoble cedex 9, France

**Matthew A. Marcus and Sirine Fakra.** Advanced Light Source (ALS), Lawrence Berkeley National Lab, MS 6-100, Berkeley, CA 94720, USA

**Emiko Harada and Yong-Eui Choi.** Division of Forest Resources, College of Forest Sciences, Kangwon National University, Chunchon 200-701, Kangwon-do, Korea

**Sébastien Pairis.** Institut Néel CNRS-UJF, Dept. Matière Condensée, Matériaux et Fonctions, Pôle Instrumentation (Microscopie Electronique), 25 av. des Martyrs, BP 166, 38042 Grenoble cedex 9, France

<sup>1</sup> Corresponding author. Email: [geraldine.sarret@ujf-grenoble.fr](mailto:geraldine.sarret@ujf-grenoble.fr)

Tel: (33) 4 76 82 80 21, Fax: (33) 4 76 82 81 01

## Abstract

Tobacco (*Nicotiana tabacum* L. cv. Xanthi) plants exposed to toxic levels of zinc and cadmium excrete metals through their leaf trichomes (epidermal hairs) as Zn,Ca- and Cd,Ca-containing grains. Little is known about the nature and formation mechanism of these precipitates. The chemical, crystalline, and non-crystalline compositions of individual grains produced by tobacco were studied by scanning electron microscopy coupled with energy dispersive X-ray analysis (SEM-EDX), micro-X-ray diffraction ( $\mu$ XRD) and calcium K-edge micro X-ray absorption near edge structure ( $\mu$ XANES) spectroscopy. Zinc is predominantly incorporated in calcite, and cadmium in calcite and vaterite. Aragonite, which occurs occasionally, does not seem to contain trace metals. In addition to being precipitated in its three possible polymorphic forms, calcite, aragonite and vaterite, calcium also is speciated as amorphous  $\text{CaCO}_3$  and possibly organic Ca in some grains. Most often, a particular grain consists of two or more crystalline and non-crystalline phases. The observed variability of intra- and inter-grain elemental and phase composition suggests that this biomineralization process is not constrained by biological factors, but instead results from thermodynamically and kinetically controlled reactions. This study illustrates the potential of laterally resolved X-ray synchrotron radiation techniques ( $\mu$ XRD and  $\mu$ XANES) to study biomineralization and metal immobilization processes in plants.

**Keywords:** biomineralization, detoxification, micro-XANES, micro-XRD.

## Introduction

Recently, a novel original mechanism of Zn and Cd detoxification was described in tobacco (*Nicotiana tabacum* L. cv. Xanthi). Tobacco exposed to Cd excreted Cd,Ca-containing grains through leaf trichomes (1, 2), and a similar excretion of Zn,Ca-containing grains was observed under Zn exposure (3). Trichomes are specialized epidermal structures. In tobacco, they are glandular and excrete various organic substances including nicotine and resins. Such detoxification process may have implication in human health since smoking is one of the principal routes of exposure to heavy metals, and also in phytoremediation as tobacco is a candidate species for phytoextraction.

The morphology, elemental composition, mineralogy as well as Zn and Cd speciation in the grains were investigated by scanning electron microscopy coupled with energy dispersive X-ray analysis (SEM-EDX), micro-X-ray fluorescence ( $\mu$ XRF), micro-X-ray diffraction ( $\mu$ XRD), Zn K-edge micro extended X-ray absorption fine structure ( $\mu$ EXAFS) (3) and Cd L<sub>III</sub> edge micro X-ray absorption near edge structure ( $\mu$ XANES) spectroscopy (Isaure et al., in prep.). Calcium was always the major component.  $\mu$ XRD analyses revealed the presence of calcite, and less frequently vaterite and aragonite, two other CaCO<sub>3</sub> polymorphs. Calcium oxalate mono and dihydrate were found occasionally. Calcite and vaterite were substituted by cations, probably Zn, Cd and possibly Mn and Mg. Zn  $\mu$ EXAFS confirmed the occurrence of Zn-substituted calcite, and evidenced Zn associations with other phases including organic compounds, silica and phosphate (3). Cd  $\mu$ XANES showed that cadmium was a Ca substituent in calcite and vaterite and/or sorbed on the surface of these minerals (Isaure et al., in prep.).

The mechanism of formation of these grains remains unclear. Biogenic minerals may result from a controlled biomineralization process leading to well defined minerals and shapes. They may also be “biologically induced”, which means that an organism promotes the precipitation, but does not control the crystallization process (4). In the present case, grains could result from the exudation of a liquid containing the various metals and substances, and precipitation of the various solid phases due to water evaporation. Alternatively, they might be formed intracellularly and excreted thereafter as suggested by Choi et al. (5). The purpose of this study is to better characterize the structure and composition of the grains. Grains excreted by tobacco under various Zn, Cd and Ca exposure conditions were investigated by SEM-EDX,  $\mu$ XRD and Ca K-

edge  $\mu$ XANES spectroscopy. Results of these complementary approaches are compared, and a hypothesis for the formation of the grains is proposed in light of these data.

## **Experimental**

### *Materials*

Plant culture and grain collection procedure have been described previously (3). Briefly, tobacco plants were grown in hydroponic conditions and exposed for 5 weeks to Zn or Cd, with or without a supplement of Ca (Table 1). A control condition with Ca only was also tested. Then, grains were collected by washing the leaves in ultrapure water and centrifugating the suspension. Several Ca-containing reference compounds were used for the Ca XANES data analysis.

Calcite, vaterite and Cd-containing vaterite were synthesized at room temperature according to a modified protocol of Paquette and Reeder (6, 7). Briefly, an aqueous solution (500 mL) containing 10 mM  $\text{CaCl}_2$  and 1.8 M  $\text{NH}_4\text{Cl}$  was placed in a glass reactor, an EPPENDORF tube containing solid ammonium carbonate was allowed to float at the surface of the solution, and the reactor was closed and kept unstirred.  $\text{NH}_4\text{Cl}$  was used as a background electrolyte to provide a high ionic strength. Initial pH was 4.9. The decomposition of ammonium carbonate produces  $\text{NH}_3(\text{g})$  and  $\text{CO}_2(\text{g})$ , which dissolve into the solution, simultaneously increasing pH and alkalinity. The supersaturation of the solution induces the formation and growth of  $\text{CaCO}_3$  crystals. Continuous sublimation of  $\text{NH}_3(\text{g})$  buffers the solution around pH = 7.9. After 13 days, the reactor contained rhombohedral crystals and spherical particles attached on the surface of the glass. The two types of particles were separated and characterized by XRD. Rhombohedral crystals corresponded to calcite, and spherical particles to vaterite. For the synthesis of Cd-containing vaterite, the same procedure was used except that after 13 days, when crystal size amounted to 150-200  $\mu\text{m}$  in diameter, the  $\text{CaCl}_2$ - $\text{NH}_4\text{Cl}$  solution was progressively doped with 0.1 M  $\text{CdCl}_2$  to a total concentration of 100  $\mu\text{M}$  Cd in order to incorporate Cd as a Ca substituent in vaterite (6, 7). The progressive addition of  $\text{CdCl}_2$  kept the solution undersaturated with respect to otavite ( $\text{CdCO}_3$ ). After 7 days, the particles were collected and separated. Spherical particles were identified as Cd-containing vaterite by XRD and  $\mu\text{XRF}$ . The Cd content was a few tens ppm based on  $\mu\text{XRF}$  analysis.

Aragonite was a natural specimen. The XANES spectrum for synthetic amorphous  $\text{CaCO}_3$  was provided by Y. Politi (8). Ca oxalate monohydrate (whewellite) was purchased from Aldrich. A

solution containing 0.5 M  $\text{Ca}(\text{NO}_3)_2$  at pH 2.6 was used as a reference for aqueous  $\text{Ca}^{2+}$ . The phase purity of all crystalline samples was checked by XRD prior to XANES analysis.

#### *Electron microscopy*

The morphology and the chemical composition of the grains were studied by SEM-EDX using a Jeol-JSM 840A equipped with a Kevex Si(Li) detector. The chamber pressure was  $10^{-6}$ - $10^{-5}$  Torr, and the accelerating voltage 20 kV. Grains were mounted on kapton tape or on carbon tape, then fixed on carbon stubs and coated with carbon. Images were taken at a magnification of 500 to 10000. EDX spectra were recorded on prominent spots of the grains to optimize the detection.

#### *Micro-XRF, $\mu$ XRD and $\mu$ XANES*

The  $\mu$ XRF,  $\mu$ XRD and Ca K-edge  $\mu$ XANES measurements were performed on beamline 10.3.2 of the Advanced Light Source (ALS, Berkeley, CA) (9). The grains were spread on kapton tape and analyzed at room temperature and pressure. First, each grain was mapped by  $\mu$ XRF. Then,  $\mu$ XANES and  $\mu$ XRD and data were recorded on the Zn-richest region for the Zn and Zn + Ca treatments, on the Cd-richest region for the Cd and Cd + Ca treatment, and on the Ca-richest region for the Ca treatment.  $\mu$ XRF data were collected at 10 keV with a beam size of  $5 \times 5 \mu\text{m}$ . The same X-ray spot size was used for Ca  $\mu$ XANES. Fluorescence X-ray yield was measured with a 7-element Ge solid-state detector. The spectra were recorded between 3900 to 4400 eV.  $\mu$ XRD patterns were recorded at an incident energy of 17 keV with a beam size of  $16 \times 7 \mu\text{m}$ . More experimental details are given in (3). Ca XANES reference spectra were recorded at room temperature on beamline ID21 at the European Synchrotron Radiation Facility (ESRF, Grenoble, France). Each spectrum is the average of two to three spectra, each about 15 minutes long.

#### *XRD and XANES data treatment*

The XRD data treatment was performed as described previously (3). Briefly, after calibration with alumina, two dimensional XRD patterns were integrated to one-dimensional patterns for peak assignment. For substituted calcite crystals, the unit cell parameters  $a$  and  $c$  were refined, and the stoichiometry of the substituent was estimated from these two parameters using the Vegard law (10) with calcite, smithsonite ( $\text{ZnCO}_3$ ) and otavite ( $\text{CdCO}_3$ ) as end-members for the Ca-Zn and Ca-

Cd solid solutions. This approach cannot be used for substituted vaterite because of the absence of a  $\text{CdCO}_3$  structural analogue of vaterite.

XANES spectra were processed using WinXAS (11). All spectra were energy calibrated with respect to calcite (inflection point for this reference set to 4042.6 eV). The collected scans were averaged; background subtracted and normalized using linear (pre-edge) or cubic (post-edge) polynomials. XANES spectra were then fitted by linear combinations using calcite, aragonite, vaterite, Cd-containing vaterite, amorphous  $\text{CaCO}_3$ , aqueous  $\text{Ca}^{2+}$  and Ca oxalate monohydrate reference spectra. The quality of the fits was quantified by the normalized sum-squares residuals  $NSS = \sum (\mu_{\text{experimental}} - \mu_{\text{fit}})^2 / \sum (\mu_{\text{experimental}})^2 \times 100$ , in the 4000-4150 eV range, where  $\mu$  is the normalized absorbance. An energy shift of  $\pm 0.5$  eV maximum and a correction of slope were allowed to account for the energy resolution of the monochromator and for possible inconsistencies in data processing. For some spectra, linear combination (LC) fitting did not provide satisfactory results, and over-absorption effects were suspected based on the comparison of these spectra with the standards. Therefore, each spectrum was fitted with and without a correction of over-absorption using a simple model (12). This model assumes that the smooth part of the resonant absorption is a constant fraction of the non-resonant background (which is a reasonable assumption in the XANES region) and that the sample is infinitely thick, *i.e.*, totally absorbs the incident beam (which is probably true considering the energy range and the size and global composition of the grains). The equation used is:

$$y_{\text{experimental}} = (1 + a) / (1 + a \cdot y_{\text{corrected}}) \quad (1)$$

where  $y$  is the normalized resonant absorbance, which equals 0 below the edge and oscillates around 1 above the edge, and  $a = \mu_{\text{resonant}} / (\mu_{\text{non resonant}} + \mu_{\text{fluorescence}})$

where  $\mu_{\text{resonant}}$ ,  $\mu_{\text{non resonant}}$  and  $\mu_{\text{fluorescence}}$  are the three components of the absorbance  $\mu$ .

Equation (1) can be solved as:

$$y_{\text{corrected}} = y_{\text{experimental}} / (1 + a (1 - y_{\text{experimental}})) \quad (2)$$

The over-absorption parameter  $a$  equals 0 in the absence of over-absorption effect, and increases with this effect. Because of the sample heterogeneity, the precise composition of the sample is not known, so  $a$  is an adjusted parameter.

## Results

The morphology of the grains as observed by SEM varied considerably. The grains varied from 10  $\mu\text{m}$  to 150  $\mu\text{m}$  in diameter. Each grain is an aggregate of different types of particles. The first type is micro faceted crystallites (Insets in Fig. 1a and 1b) and the second type is globular structures of various sizes (from 2 to 50  $\mu\text{m}$ , Fig. 1c, 1d and 1e). Some grains such as Zn<sub>2</sub> (Fig. 1c) seem visually less crystalline. The elemental composition of the grains varies from one grain to another, and within the same grain. Ca was always the major component regardless of the plant metal treatment conditions. Minor elements include Mg, Si, P, Cl, K, and Zn or Cd depending on the plant treatment (Fig. 1). The high Si peaks observed in Fig. 1a to 1d are attributed to kapton tape on which the grains were mounted. Silicon is not detected in the grain presented in Fig. 1e (mounted on carbon tape). However, Si was found in small amount in some grains (not presented in this study), as well as Mn.

Our previous study using  $\mu\text{XRD}$  (3) showed that grain ZnCa<sub>3</sub> contained substituted calcite and aragonite, that grain ZnCa<sub>4</sub> contained substituted calcite, and that grain Zn<sub>2</sub> did not contain crystalline phases. The two-dimensional  $\mu\text{XRD}$  patterns for grains ZnCa<sub>5</sub> and Zn<sub>3</sub> show that the Bragg reflections for these two grains consist of small arcs of Debye-Scherrer rings, indicating that the grains are composed of micrometer-size mosaic crystals (Fig. 2b). All reflections correspond to substituted calcite, and the major Ca substituent is Zn based on  $\mu\text{XRF}$  (Fig. 2a). Note that although Ca is the major element, the Ca  $K\alpha$  peak has a low intensity relative to the Zn  $K\alpha$  peak due to air absorption and the lower fluorescence yield of Ca vs. Zn. The refined unit cell parameters  $a$  and  $c$  for grain ZnCa<sub>5</sub> and Zn<sub>3</sub> were 4.97 and 16.97  $\text{\AA}$ , and 4.95 and 16.83  $\text{\AA}$ , respectively, compared to 4.9896 and 17.0610  $\text{\AA}$  for pure calcite. The calculated formulae using the Vegard law were  $\text{Ca}_{0.95}\text{Zn}_{0.05}\text{CO}_3$  and  $\text{Ca}_{0.89}\text{Zn}_{0.11}\text{CO}_3$ , respectively. The difference in the Zn stoichiometry coefficient obtained using parameters  $a$  and  $c$  was  $\pm 0.01$ . The  $\mu\text{XRD}$  results for the Cd-containing grains will be presented separately together with Cd  $L_{\text{III}}$ -XANES data (Isaure et al., in preparation). Briefly, the grains CdCa<sub>2</sub> and Cd<sub>10</sub> contain micrometer crystals of substituted calcite and finer (nanometer sized) crystals of substituted vaterite. Grain CdCa<sub>3</sub> contains nano-crystals of substituted vaterite only. Finally, no crystalline phases were detected in grain CdCa<sub>6</sub>. For Cd- substituted calcite, the Vegard law provides an imprecise estimation of Cd stoichiometry because the contrast in ionic radius between Cd and Ca is small (0.95  $\text{\AA}$  for  $\text{Cd}^{2+}$  and 1.00  $\text{\AA}$  for  $\text{Ca}^{2+}$  compared to 0.74  $\text{\AA}$  for  $\text{Zn}^{2+}$ ) (13). For instance, the substitution rate for grain CdCa<sub>2</sub> could be anywhere between 30 and 80%. It was not possible to calculate the

stoichiometry of Cd in vaterite because of the absence of a Cd end member (see the Experimental section).

Calcium being the major element in the grains, Ca K-edge  $\mu$ XANES spectroscopy was then performed to get some insights on the composition of the grains, and test for the presence of amorphous Ca phases. Figure 3a shows the XANES spectra for several Ca reference compounds. The four  $\text{CaCO}_3$  species (calcite, vaterite, aragonite and amorphous  $\text{CaCO}_3$  (ACC)) have clearly distinct spectra, which enables their identification (14, 15). However, Ca XANES has no sensitivity to substitutional impurities as seen for instance for low Cd-containing vaterite (Cd content lower than 1%, as estimated by  $\mu$ XRF) and pure vaterite exhibiting nearly identical spectra. The spectra for aqueous  $\text{Ca}^{2+}$ , Ca oxalate monohydrate and ACC share some similarities. However, the lower part of the edge is shifted to lower energy for ACC spectrum, and the maximum of the white line (zero value of the first derivative) increases from 4049.5 eV (ACC) to 4049.9 eV (Ca oxalate monohydrate) and to 4050.5 eV (aqueous  $\text{Ca}^{2+}$ , Fig. 3b). The aragonite spectrum is distinct from the three previous spectra in displaying a shoulder at 4046 eV (arrow in Fig. 3), and a minimum between 4060 and 4070 eV.

Figure 4 shows the Ca  $\mu$ XANES spectra for the grains. They were fitted by LC using the standard spectra presented above, and results are presented in Table 2. The ZnCa3 spectrum presents strong similarities with the aragonite spectrum, but markedly lower amplitude. The drop in amplitude suggests some over-absorption effect (12) due to a high Ca content of the analyzed spot. The fit without over-absorption correction (see materials and Methods) did not provide satisfactory result ( $NSS = 0.065$  %, with 68% vaterite + 25% aragonite). Introducing an over-absorption correction greatly improved the fit ( $NSS = 0.014$  % with aragonite as only component, Fig. 4). The  $a$  value found (1.38) corresponds to a very strong over-absorption effect. The fit was not improved significantly by introducing a second component ( $NSS$  decreased by less than 10%). Thus, the spot analyzed by  $\mu$ XANES likely contains aragonite as the sole Ca species. The grains ZnCa4 and ZnCa5 were fitted with 98% calcite. The fit was slightly improved with a correction of over-absorption ( $NSS = 0.015$  and  $0.021$  %, compared to  $0.020$  and  $0.035$  %, respectively), and the proportions were unchanged. Adding a second component did not improve significantly the fits ( $NSS$  decreased by less than 10%).

For grain Zn2 and CdCa6, fits without over-absorption correction were not satisfactory ( $NSS = 0.048$  and  $0.091$  %, respectively, for two-component fits). Fair one-component fits with over-



absorption correction were obtained with ACC ( $NSS = 0.021$  and  $0.024$  %, respectively), but the match was not optimal for the first oscillation (around  $4080$  eV). Ca oxalate monohydrate and aqueous  $Ca^{2+}$  provided weaker fits ( $NSS = 0.086$  and  $0.053$  % for Zn2, and  $0.076$  and  $0.043$  % for CdCa6, respectively). Adding a second component did improve the reproduction of the first oscillation. Several fits of equivalent qualities were obtained with ACC as major component (about  $80$  and  $70$  % of total Ca) and various species as secondary component.  $NSS$  values were more than doubled if ACC was excluded (Table 2 and Fig. 1 in Supplemental Information). Therefore, grains Zn2 and CdCa6 likely contain ACC as major species, and an additional species whose nature remains unknown.

For the other grains (Zn3, CdCa2, CdCa3 and Cd10), over-absorption correction did not improve the fits. Calcite was the major form in grains Zn3 and CdCa2, and fits of equivalent quality were obtained with ACC, aqueous  $Ca^{2+}$  and Ca oxalate monohydrate as minor species. Aqueous  $Ca^{2+}$  is unlikely in solid-state material. ACC and Ca oxalate monohydrate are more likely. In the absence of reference spectra for Ca bound to organic ligands other than oxalate, this latter compound may be considered as a proxy for Ca bound to organic compounds in general. Therefore, this pool is referred to as “organic Ca and/or ACC” in Table 3. Vaterite was found in grains CdCa3 and Cd10. For this latter grain only, no satisfactory fit was obtained with two components ( $NSS = 0.046$  %), so a third component was introduced. Again, a contribution of organic Ca and/or ACC was found in grains CdCa3 and Cd10.

The speciation of Ca was then compared with the mineralogy and morphology of the grains (Table 3). The percentages were rounded to the nearest ten for clarity. Except for two grains, ZnCa3 and CdCa2, the same crystalline species were identified by  $\mu$ XRD and Ca  $\mu$ XANES. Zn-substituted calcite and Cd-substituted vaterite were identified by  $\mu$ XRD in grains ZnCa3 and CdCa2, respectively, but not by Ca  $\mu$ XANES spectroscopy. This difference likely results from the larger beam size and higher penetration depth of X-rays in XRD measurements relative to  $\mu$ XANES ( $16 \times 7$   $\mu$ m vs  $5 \times 5$   $\mu$ m, and a few tens of  $\mu$ m at  $17$  keV vs. a few  $\mu$ m at  $4$  keV). Thus, XRD probes a different material volume than Ca  $\mu$ XANES even when conducted on the same spot.

## Discussion and Conclusion

Results showed that beside crystalline calcium carbonates (calcite, vaterite and aragonite), the tobacco grains contained ACC as well. Whewellite (Ca oxalate monohydrate) did show up in some XANES fits, but its presence could not be firmly attested. Ca oxalate mono- and dihydrate have several XRD peaks in common with calcite, but peaks at distinct positions as well. These two minerals were positively identified by  $\mu$ XRD in other tobacco grains based on the presence of these specific peaks (3). In the present study, no such peaks were found on the XRD patterns. However, it is still possible that coarse crystals of Ca oxalate mono or dihydrate are present but produce non-specific peaks only, or that Bragg conditions were not met for these coarse crystals. Therefore, the presence of Ca oxalate mono- and dihydrate cannot be ruled out. Other undetermined organic ligands may also complex Ca. In addition, mixed mineral and organic Ca compounds such as organic matter-containing calcite (16) may occur.

The Ca  $\mu$ XANES analysis showed that strong over-absorption effects may take place and decrease dramatically the amplitude of the spectra. We show that this effect is far from negligible when identifying and quantifying Ca species. For instance, for grain ZnCa3, the uncorrected spectrum was fitted by 68% vaterite + 25% aragonite, and the corrected spectrum was fitted with 100% aragonite. Note that the LCF without over-absorption correction was relatively bad, which alerted us on the possibility of an over-absorption effect.

In the environment, ACC is thermodynamically unstable and rapidly transforms into vaterite and then calcite (17). However, it is found as a stable compound in plants (e.g., cystoliths) and animals (e.g., cuticle of crustaceans, spicules of ascidia, granules in molluscs) (18). ACC is probably stabilized by proteins, magnesium and phosphorus in these organisms (18). In our case, Mg and P were found in the grains.

Biologically controlled biomineralization leads to well defined mineral species and shapes. Here, the variety of morphologies and of  $\text{CaCO}_3$  crystal structures, and their coexistence with amorphous and possibly organic forms, supports the hypothesis of a biologically induced (as opposed to biologically controlled) biomineralization. This study illustrates the potential of microfocused X-ray techniques to study biomineralization processes, and strategies of metals immobilization developed by plants to cope with metal toxicity.

## Acknowledgements

265 We acknowledge the ALS (Berkeley, USA) and the ESRF (Grenoble, France) for the provision  
266 of beamtime. We are grateful to Jean Susini and the staff of beamline ID21 at the ESRF for their  
267 technical support during the experiment. The operations of the Advanced Light Source at  
268 Lawrence Berkeley National Laboratory are supported by the Director, Office of Science, Office  
269 of Basic Energy Sciences, Materials Sciences Division, of the US Department of Energy under  
270 Contract No. DE-AC02-05CH11231. We acknowledge Y. Politi and S. Weiner for sharing the  
271 ACC Ca XANES spectrum, and two anonymous reviewers.

## References

1. Choi, Y. E., Harada, E., Wada, M., Tsuboi, H., Morita, Y., Kusano, T. & Sano, H. *Planta* **213**, 45-50 (2001).
2. Choi, Y. E., Harada, E., Kim, G. H., Yoon, E. S. & Sano, H. *J. Plant Biol.* **47**, 75-82 (2004).
3. Sarret, G., Harada, E., Choi, Y. E., Isaure, M. P., Geoffroy, N., Birschwilks, M., Clemens, S., Fakra, S., Marcus, M. A. & Manceau, A. *Plant Physiol.* **141**, 1021-1034 (2006).
4. Lowenstam, H. & Weiner, S. *On Biomineralization* (Oxford University Press, New York, Oxford, 1989).
5. Choi, Y. E. & Harada, E. *J. Plant Biol.* **48**, 113-119 (2005).
6. Paquette, J. & Reeder, R. J. *Geochim. Cosmochim. Acta* **59**, 735-749 (1995).
7. Reeder, R. J. *Geochim. Cosmochim. Acta* **60**, 1543-1552 (1996).
8. Politi, Y., Levi-Kalishman, Y., Raz, S., Wilt, F., Addadi, L., Weiner, S. & Sagi, I. *Adv. Funct. Mat.* **16**, 1289-1298 (2006).
9. Marcus, M. A., MacDowell, A. A., Celestre, R., Manceau, A., Miller, T., Padmore, H. A. & Sublett, R. E. *J. Synchrotron Rad.* **11**, 239-247 (2004).
10. West, A. *Solid State Chemistry and its Applications* (Wiley, New York, 1984).
11. Ressler, T. *J. Phys. IV* **7**, c2-269 (1997).
12. Manceau, A., Marcus, M. A. & Tamura, N. in *Applications of Synchrotron Radiation in Low-Temperature Geochemistry and Environmental Science* (eds. Fenter, P., Rivers, M., Sturchio, N. & Sutton, S.) 341-428 (Reviews in Mineralogy and Geochemistry, Mineralogical Society of America, Washington, DC., 2002).
13. Shannon, R. D. *Acta Crystallogr. A* **32**, 751-767 (1976).
14. Levi-Kalishman, Y., Raz, S., Weiner, S., Addadi, L. & Sagi, I. *Adv. Funct. Mat.* **12**, 43-48 (2002).
15. Pattanaik, S. *Nucl. Inst. Meth. Phys. Res. B* **229**, 367-374 (2005).
16. Phillips, B. L., Lee, Y. J. & Reeder, R. J. *Environ. Sci. & Technol.* **39**, 4533-4539 (2005).
17. Ogino, T., Suzuki, T. & Sawada, K. *J. Cryst. Growth* **100**, 159-67 (1990).
18. Weiner, S., Levi-Kalishman, Y., Raz, S. & Addadi, L. *Connective Tissue Research* **44 Suppl. 1**, 214-218 (2003).

**Table 1.** Tobacco culture conditions and name of the grains investigated

Treatment conditions	Cation Concentrations in the Nutrient Solution (mM)			Grain Names	Techniques and References				
	Ca	Zn	Cd		SEM-EDX	$\mu$ XRD	Zn $\mu$ EXAFS	Cd $\mu$ XANES	Ca $\mu$ XANES
Zn	0.28	0.25	0	Zn2	(3) and this paper	(3)	(3)	-	this paper
				Zn3	-	this paper	unpubl.	-	
Zn + Ca	3.28	0.25	0	ZnCa3	(3) and this paper	(3)	(3)	-	this paper
				ZnCa4	(3) and this paper	(3)	(3)	-	this paper
				ZnCa5	-	this paper	unpubl.	-	this paper
Cd	0.28	$0.08 \cdot 10^{-3}$	0.025	Cd10	(a)	(a)	-	(a)	this paper
Cd + Ca	3.28	$0.08 \cdot 10^{-3}$	0.025	CdCa2	(a)	(a)	-	(a)	this paper
				CdCa3	(a)	(a)	-	(a)	this paper
				CdCa6	(a)	(a)	-	(a)	this paper
Ca	3.28	$0.08 \cdot 10^{-3}$	0	Ca3	this paper	-	-	-	-

(a) Isaure et al., in prep.

**Table 2. Ca  $\mu$ XANES Results**

Treatment	Grain Name	$a^1$	Proportion of Ca species (%) Determined by Linear Combination							
			Fitting the $\mu$ XANES Spectra					Sum	NSS (%) <sup>2</sup>	
			Calcite	Vaterite	Aragonite	Amorphous CaCO <sub>3</sub>	Aqueous Ca <sup>2+</sup>			Ca oxalate 1 H <sub>2</sub> O
Zn+Ca	ZnCa3	1.38			97 ± 2				97	0.014 <sup>3</sup>
	ZnCa4	0.12	98 ± 2						98	0.015 <sup>3</sup>
	ZnCa5	0.17	98 ± 2						98	0.021 <sup>3</sup>
Zn	Zn2	0.27			22 ± 10	76 ± 15			97	0.011 <sup>3</sup>
		0.27				77 ± 15		20 ± 15	97	0.016
		0.27				79 ± 15	17 ± 15		96	0.019
		0.42				(excluded)	55 ± 15	45 ± 15	100	0.050
	Zn3		62 ± 5			29 ± 5			91	0.009 <sup>3</sup>
			70 ± 5					22 ± 5	92	0.016
			71 ± 5				21 ± 5		92	0.018

Cd+Ca	CdCa2		85 ± 5		13 ± 5		98	0.012 <sup>3</sup>	
			87 ± 5			10 ± 5	97	0.014	
			89 ± 5		9 ± 5		98	0.015	
	CdCa3		77 ± 5		21 ± 7		98	0.031 <sup>3</sup>	
			79 ± 5			20 ± 7	99	0.036	
			82 ± 5		16 ± 7		98	0.037	
	CdCa6	0.38			74 ± 15		25 ± 15	99	0.015 <sup>3</sup>
		0.42			68 ± 15	32 ± 15		100	0.019
		0.28			(excluded)	73 ± 15	25 ± 15	98	0.040
	Cd	Cd10	29 ± 7	42 ± 8		25 ± 5		96	0.022 <sup>3</sup>
			25 ± 7	37 ± 8		34 ± 5		96	0.025
			28 ± 7	42 ± 8			26 ± 5	96	0.028

---

<sup>1</sup> Coefficient of over-absorption. <sup>2</sup> Residual between fit and experimental data  $NSS = \Sigma(\mu_{\text{experimental}} - \mu_{\text{fit}})^2 /$

$\Sigma(\mu_{\text{experimental}})^2 \times 100$  in the 4000-4150 eV range, where  $\mu$  is the normalized absorbance. <sup>3</sup> Fit shown in Fig. 4. The error bars on the percentages correspond to the variation needed to increase  $NSS$  by 20%.

**Table 3. Summary of the information obtained on each grain<sup>1</sup>**

<b>Treatment</b>	<b>Grain Name</b>	<b>Ca Speciation (<math>\mu</math>XANES Results)<sup>1</sup></b>	<b>Mineralogy (<math>\mu</math>XRD Results)</b>	<b>Aspect of the Grain (SEM Results)</b>
<b>Zn+Ca</b>	ZnCa3	100% aragonite	Aragonite, Zn-subst. calcite (Ca <sub>0.93</sub> Zn <sub>0.07</sub> CO <sub>3</sub> )	faceted
	ZnCa4	100% calcite	Zn-subst. calcite (Ca <sub>0.87</sub> Zn <sub>0.13</sub> CO <sub>3</sub> )	faceted
	ZnCa5	100% calcite	Zn-subst. calcite (Ca <sub>0.95</sub> Zn <sub>0.05</sub> CO <sub>3</sub> )	not observed
<b>Zn</b>	Zn2	80% ACC + 20% undetermined	No diffraction peaks	rounded
	Zn3	70% calcite + 30% organic Ca and/or ACC	Zn-subst. calcite (Ca <sub>0.89</sub> Zn <sub>0.11</sub> CO <sub>3</sub> )	not observed
<b>Cd+Ca</b>	CdCa2	90% calcite + 10% organic Ca and/or ACC	Cd-subst. calcite, Cd-subst. vaterite	not observed
	CdCa3	80% vaterite + 20% organic Ca and/or ACC	Cd-subst. vaterite	rounded
	CdCa6	70% ACC + 30% undetermined	No diffraction peaks	not observed
<b>Cd</b>	Cd10	30% calcite + 40% vaterite +	Cd-subst. calcite,	rounded +
		30% organic Ca and/or ACC	Cd-subst. vaterite	faceted

<sup>1</sup> The error bar on the percentages varies from 5 to 15% depending on the species (see Table 2)



## Figure Captions

Figure 1: SEM imaging for the grains ZnCa3 (a), ZnCa4 (b) Zn2 (c), CdCa3 (d) and grain Ca3 (e), and EDX analyses were performed on the spots marked by a black cross.

Figure 2:  $\mu$ XRF spectrum (a) one- and two-dimensional  $\mu$ XRD patterns (b) for grain ZnCa5 and Zn3. All XRD peaks were attributed to substituted calcite. The positions of three peaks for pure calcite are indicated by arrows.

Figure 3: Ca K-edge XANES spectra for the reference compounds used in the linear combination fits (a) and zoom on the main peak for aqueous  $\text{Ca}^{2+}$ , Ca oxalate monohydrate and ACC (b).

Figure 4: Ca K-edge  $\mu$ XANES spectra for the tobacco grains and corresponding linear combination fits. Five spectra (Zn2, CdCa6, ZnCa3, ZnCa5 and ZnCa4) were corrected for over-absorption.

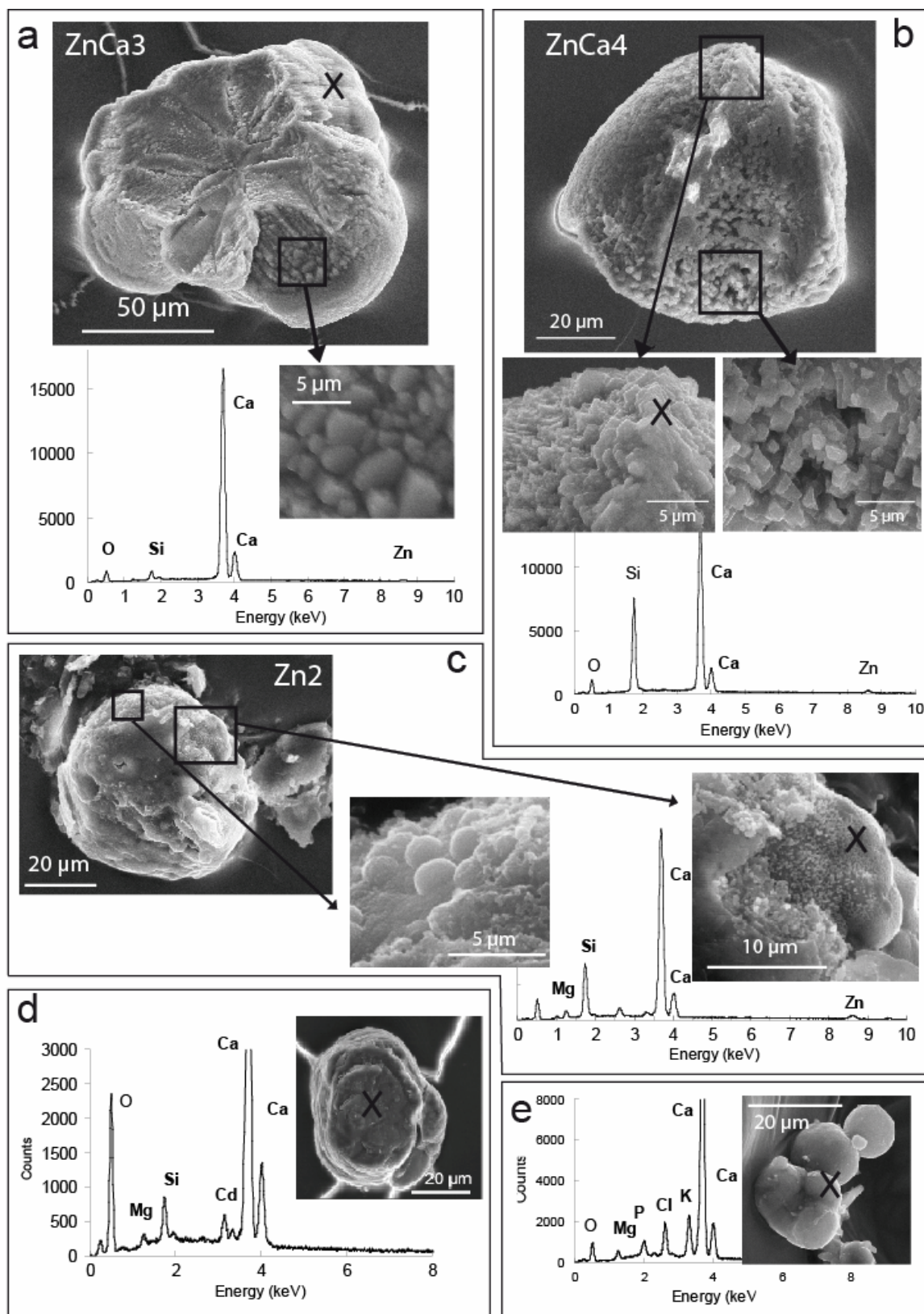


Figure 1

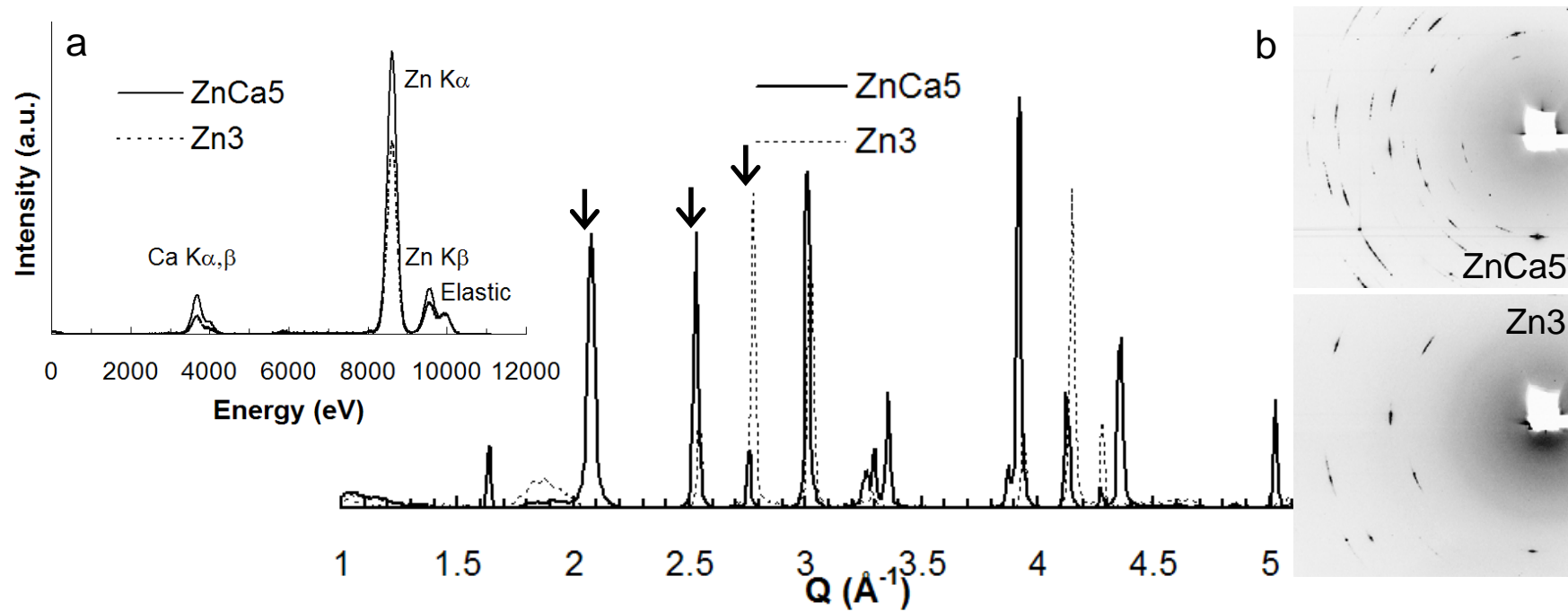


Figure 2

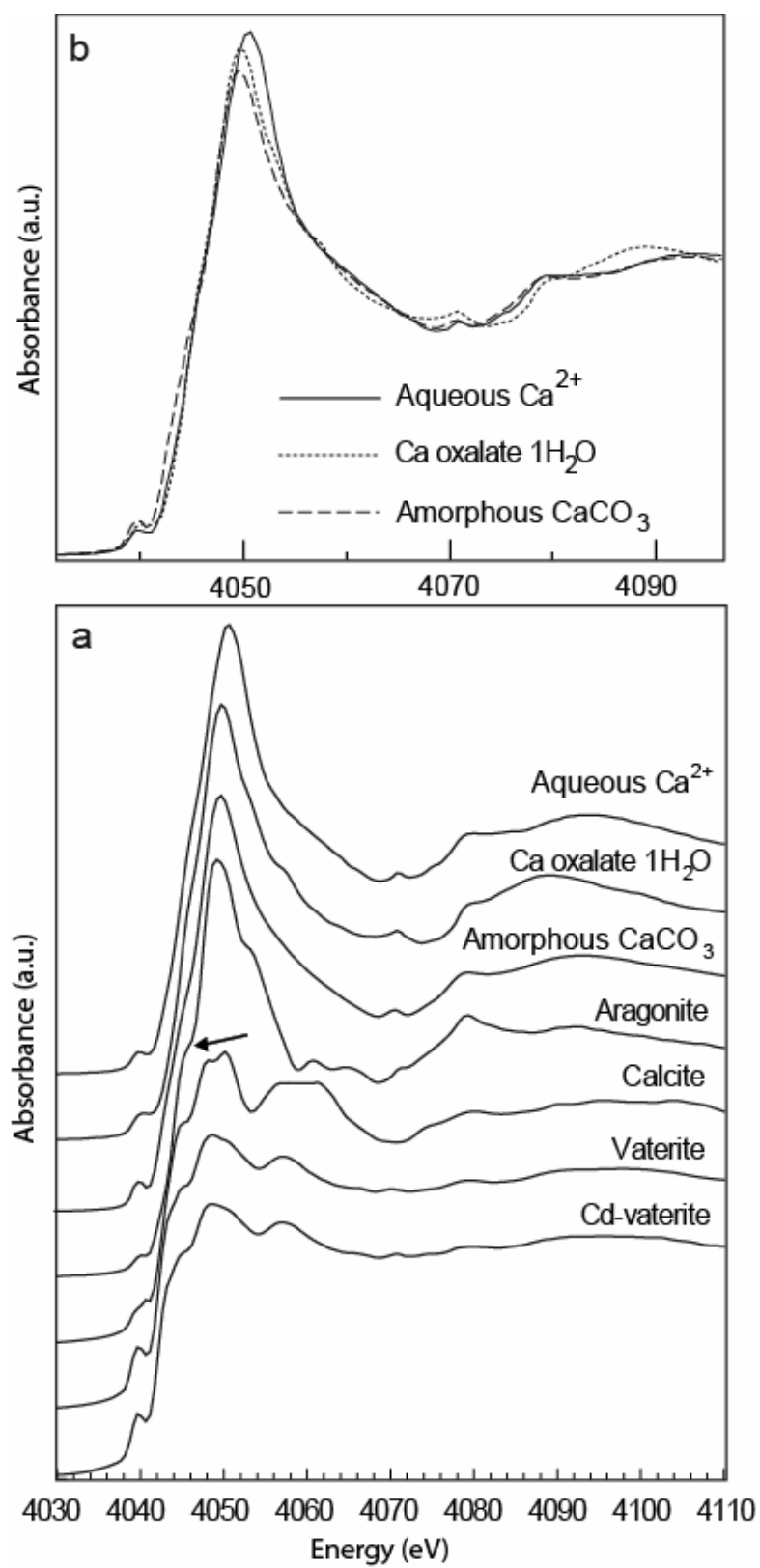


Figure 3

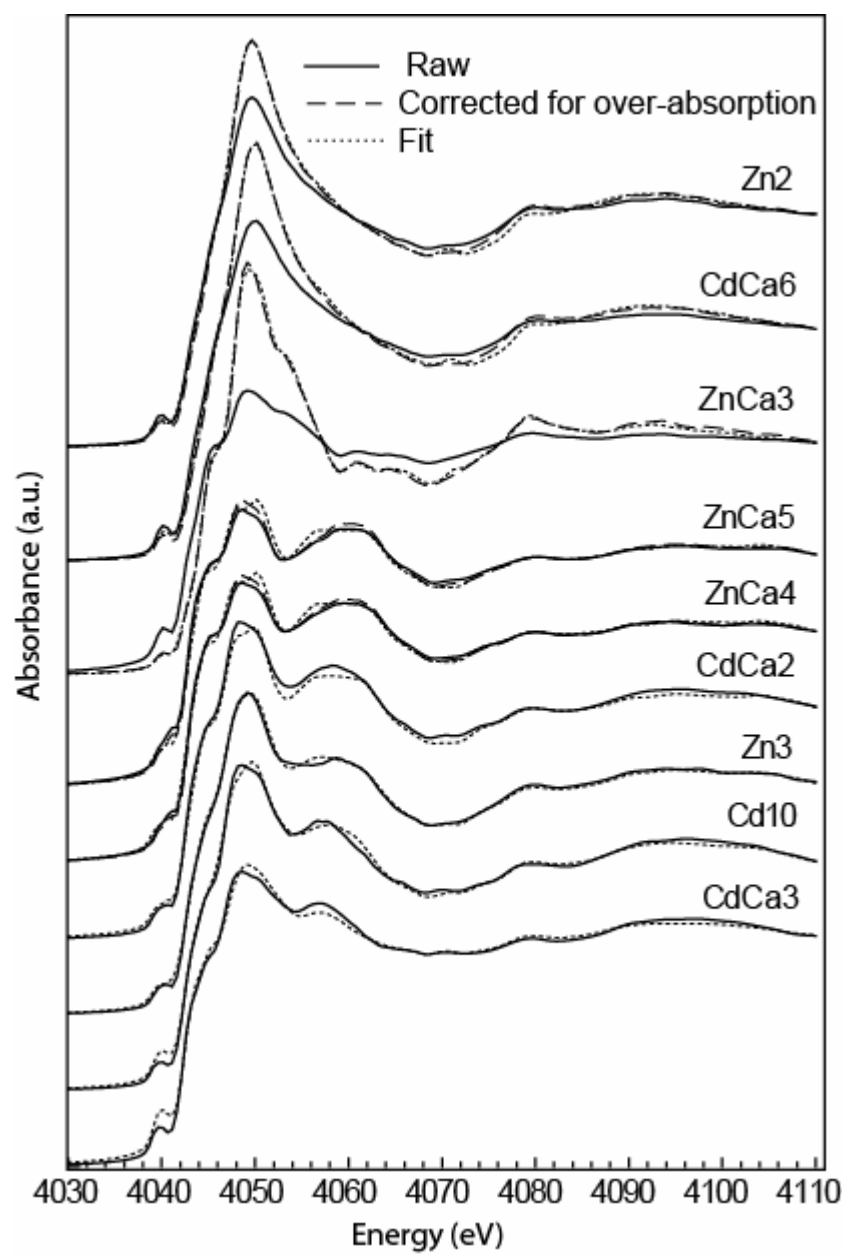


Figure 4

## Supplemental information

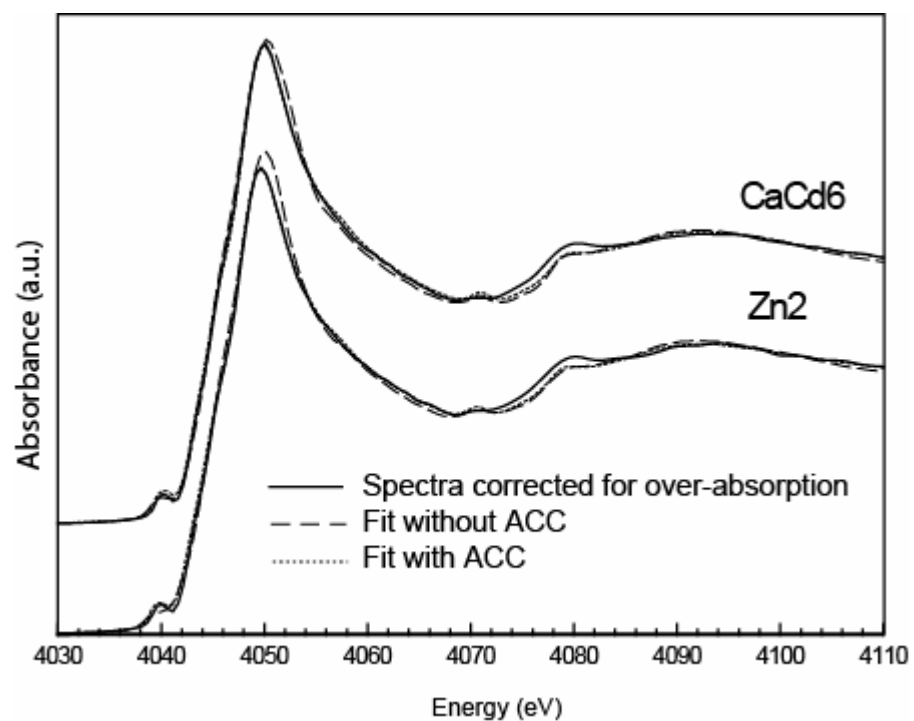


Figure 1: Comparison of the best two-component fits obtained for CaCd6 and Zn2 with and without ACC.